Xiaolong Bai, Boyuan Ban, Jingwei Li, Zhijian Peng and Jian Chen*

Distribution Behavior of B and P during Al-Si Melt Directional Solidification with Open-Ended Crucible

DOI 10.1515/htmp-2016-0127
Received June 25, 2016; accepted February 3, 2017

Abstract: Distribution behavior of B and P during directional solidification of Al-20Si, Al-30Si and Al-40Si alloys has been investigated. Macrostructure of the Al-Si alloy ingots and concentration profile of elements B and P reveal that the elements segregate to eutectic Al-Si melt during growth of primary Si flakes, and P gradually segregates to the top of the ingots during directional solidification. An apparent segregation coefficient, k_a, is introduced to describe the segregation behavior of B and P between the primary Si and the Al-Si melt and compared with thermodynamic theoretical equilibrium coefficients. The apparent segregation coefficients of B and P decrease with increase of solidification temperature.

Keywords: solvent refining, Al-Si alloy, directional solidification, apparent segregation coefficient

Introduction

Impurities removal from metallurgical-grade silicon (MG-Si) by metallurgical method to produce solar-grade silicon (SoG-Si) attract research interests [1–3]. As is well known, the content of all kinds of impurities in SoG-Si must be lower than 1 ppmw to manufacture solar cells [4]. Metallic impurities in silicon with small segregation coefficient (such as Fe, Ti, Al, and Ca) can be effectively removed by directional solidification [5] or zone refining [6], but these methods are not effective for removing impurities with large segregation coefficient, such as boron and phosphorous ($k_B = 0.8$ and $k_P = 0.35$ [7]). Solvent refining is an active method of B and P removal due to the much smaller segregation coefficients of B and P between solid Si/melt than that between solid/liquid Si [8, 9]. Fe [1], Cu [10], Ga [11], Al, etc. have been selected as the solvent to refine MG-Si for years. And studies on Al as the solvent attract the most interest of all, because solvent refining with Al-Si alloy has cheaper raw material and lower operating temperature.

Li [12, 13] reported that most of the impurities in Si can be eliminated during Al-Si solvent refining process. Nishi [14] found that the impurity elements could be efficiently removed from the silicon phases to Al-Si melt by directional solidification. And the effect of electromagnetic stirring on refinement of primary Si in hypereutectic Al-Si alloy was studied by Lu [15] and Ban [16]. Directional solidification or electromagnetic stirring force has been used to enrich primary Si phases at the bottom part of the ingots to separate the primary Si phase from the Al-Si eutectic matrix [17, 18]. Models based on the experimental results and simulation to describe the separation mechanism of the primary Si from the hypereutectic Al-Si alloy melts under alternating electromagnetic fields were presented by Xue [19]. All these indicate that high temperature, directional solidification and electromagnetic stirring contribute to the impurities removal during solvent refining. In addition, Yoshikawa [8, 9] calculated segregation coefficients of B and P in Al-Si alloys to reveal their relationship with solidification temperature. It has found that segregation coefficients of B and P decrease when solidification temperature decreases. A concept of apparent segregation coefficient was proposed by Li [20, 21] to describe removal behavior of B and P under non-equilibrium conditions in Al-Si alloys. The studies reveal that the apparent segregation coefficients of B and P are much larger than the equilibrium coefficients calculated by Yoshikawa and more applicable to practical production. Then Ban [16] reported that the apparent segregation coefficients of B and P decrease when the strength of

***Corresponding author: Jian Chen,** Key Laboratory of Novel Thin Film Solar Cells, Institute of Applied Technology, Hefei Institutes of Physical Science, Chinese Academy of Science, Hefei 230031, China, E-mail: jchen@ipp.ac.cn
Xiaolong Bai, School of Engineering and Technology, China University of Geosciences, Beijing 100083, China; Key Laboratory of Novel Thin Film Solar Cells, Institute of Applied Technology, Hefei Institutes of Physical Science, Chinese Academy of Science, Hefei 230031, China, E-mail: Xiaolong_89@163.com
Boyuan Ban, Jingwei Li, Key Laboratory of Novel Thin Film Solar Cells, Institute of Applied Technology, Hefei Institutes of Physical Science, Chinese Academy of Science, Hefei 230031, China
Zhijian Peng, School of Engineering and Technology, China University of Geosciences, Beijing 100083, China

electromagnetic stirring increases. The solidification processes of Yoshikawa's were conducted in near equilibrium conditions. Li and Ban solidified the Al-Si alloys at slow cooling rates, which took a lot of time to remove B and P. However, the distribution behavior and the apparent segregation coefficients of B and P under regular solidification rates are not clear.

In this paper, to determine distribution characteristics of B and P in Al-Si alloys, directional solidification technique was used to prepare the Al-Si ingots with an open-ended crucible during the solvent refining process, and the melt was heated and stirred by electromagnetic induction in all process (heating, holding, and solidifying). This method has the following advantages over normal directional solidification: electromagnetic stirring of the melt, reusable crucible and no pollution to the alloys. The macrostructure of the ingots and the concentration profile of B and P in primary Si flakes and eutectic Si powders were observed and tested. The apparent segregation coefficient of B and P in the Al-Si alloys solidification is then calculated. Finally, the effect of solidification temperature on the apparent segregation coefficients is comparatively studied.

Experimental

MG-Si and commercial Al were used as raw materials. The contents of the impurity elements in these materials determined by Inductively Coupled Plasma Optical Emission Spectrometry (ICP-OES) are listed in Table 1. The Al-Si alloy ingots were melted in a SPZ-25 medium-frequency induction furnace under Ar atmosphere. A schematic drawing of the furnace is shown in Figure 1.

Three alloys (Al-20Si, Al-30Si and Al-40Si) were melted and solidified under Ar atmosphere by the same process. About 1500 g raw materials of the nominal compositions were put in a graphite heater tube (80-mm I.D., 100-mm O.D., 200-mm length). Figure 2

Table 1: Impurity content in raw materials (ppmw).

Impurity element	Al	Fe	Ca	B	P	Cu	Mg
In silicon	2434	2818	37	25	43	35	8
In aluminum	Bal.	14152	111	1	26	28	60
Impurity element	Mn	Sn	V	Zn	Ti	Cr	Ni
In silicon	105	7	351	1	437	7	154
In aluminum	41	4	171	47	33	18	49

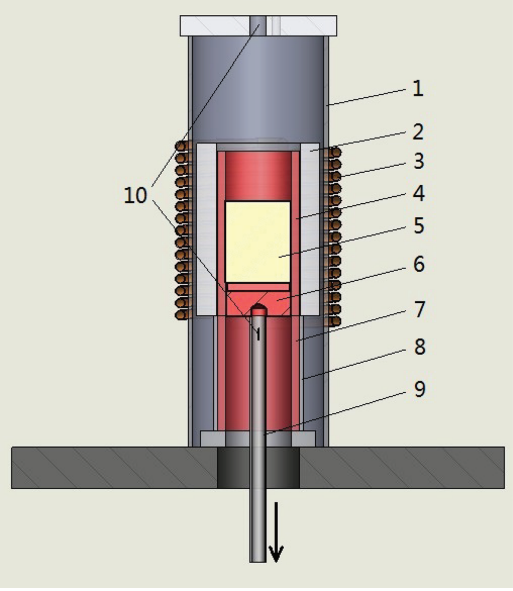

Figure 1: Schematic drawing of furnace 1 quartz tube; 2 thermal insulation tube; 3 induction coil; 4 graphite heater tube; 5 Al-Si melt; 6 graphite bottom support; 7 graphite tube; 8 quartz supporting tube; 9 stainless steel tube connected to pulling mechanism; 10 gas inlet.

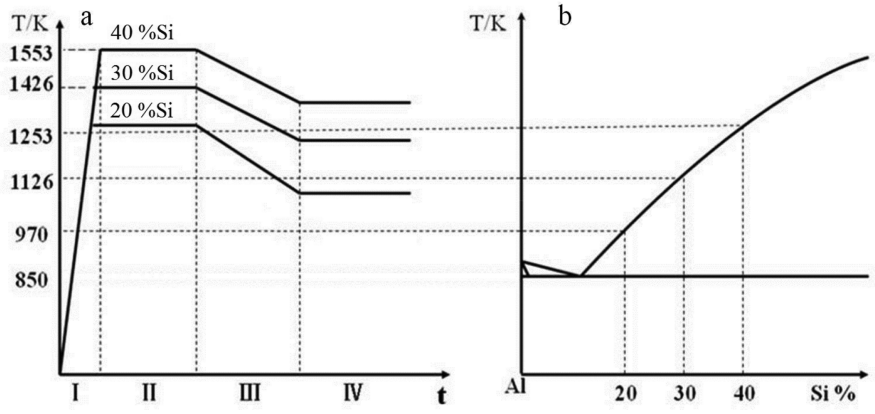

Figure 2: Temperature-time curves of different samples (a) Temperature (T) vs. time (t) curves during processing; (b) Al-Si phase diagram.

displays the temperature–time curves of the process and an Al-Si phase diagram of the alloys with different contents of Si. In step I, the graphite tube was rapidly heated up to the temperature about 300 K (°C) above the liquidus temperature of the alloy to rapidly melt the raw materials. In step II, after the Si rocks were completely melted, the temperature was held for 30 min and the melt was stirred with a quartz rod in every 5 min to ensure homogeneous mixing of the melt. Then, in step III, the power of the furnace was reduced to lower the temperature of the melt to 100 K (°C) above the liquidus of the alloy. Finally, in step IV, the sample was solidified by pulling it out of the heater tube at a rate of 3 mm/min.

The ingots were cut into two parts along their vertical axis. The cutting surface of one part was polished for macrostructure observation. A plate with 10 mm thickness was cut with a saw from the other part, and then divided into five equal bricks from the bottom to the top of the plate, which is shown in Figure 3. The obtained bricks were weighed and put in beakers with diluted hydrochloric acid to remove Al matrix by their reaction, which left behind primary Si flakes and eutectic Si powder. After the reaction was completed, the primary Si flakes and the eutectic Si powder were washed with deionized water, dried and separated. Finally the content of B and P in the primary Si flakes and the eutectic Si powder of each brick was measured by ICP-OES.

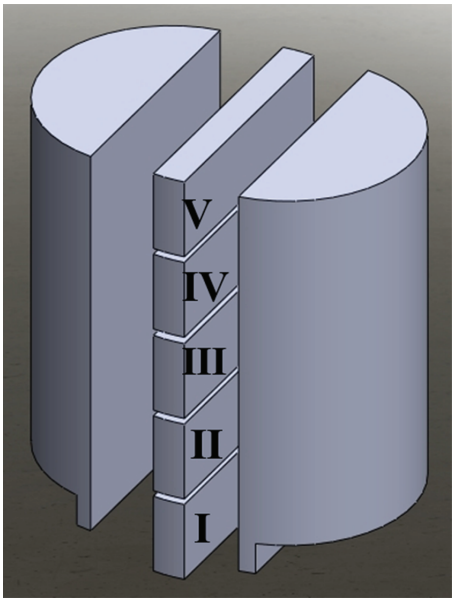

Figure 3: Sketch of cutting position of samples.

Results and discussion

Effect of directional solidification

Figure 4 shows the vertical cross-section of the ingots and the macrostructure of the marked areas. The mass fractions of the primary Si flakes in five different parts from the bottom to the top of each ingot are shown in Figure 5.

It can be seen in Figure 4 that the primary Si phases in Al-20Si (wt %) alloy are mainly in grainy shape, but the primary Si phases in Al-30Si and Al-40Si alloys are plate-like. The needle-like primary Si phases at the bottom and the edge of the ingots indicate that the nucleation commences from these areas. In Figure 5, the content of the primary Si flakes increases with increase of Si content in these three samples and decreases from the bottom to the top in each ingot, which was specifically discussed in our early publication [22]. In addition, the amount of the impurities B and P in the primary Si flakes increases from the bottom to the top as shown in Figure 6. All the above indicates the impurities removal mechanism of directional solidification: Firstly, the primary Si flakes forms at the bottom end that has lower temperature, and then the impurities are rejected to the eutectic Al-Si melt when the primary Si flakes grow. Finally, the directional solidification drives the impurities to the top of the ingots.

There are interfaces between the parts with dense and sparse primary Si phase, which are marked by dotted lines in Figure 4. The same phenomenon is shown in Figure 5, in which the mass fraction of the primary Si flakes drops at the interfaces. The part with dense primary Si phases approximately accounts for 60 % of the ingots in Al-20Si and Al-30Si and 80 % in Al-40Si. Furthermore, the distribution of the primary Si flakes in Figure 5 may be described by directional solidification theory [23]. At the beginning of the solidification, the primary Si flakes form and grow at the bottom of the ingot. When the solidification continues, the Si concentration ahead of the solid/liquid interface decreases, forming a concentration gradient. Then the fraction of the primary Si phases in the solidified part decreases until the composition of melt reaches the eutectic point. Finally, the concentration of the alloy remains at the eutectic point till the end of the solidification. However, the fraction of the primary Si phases at the top of the ingots does not reach zero in Figure 5. Many primary Si grains can be found in the top area of the ingots as

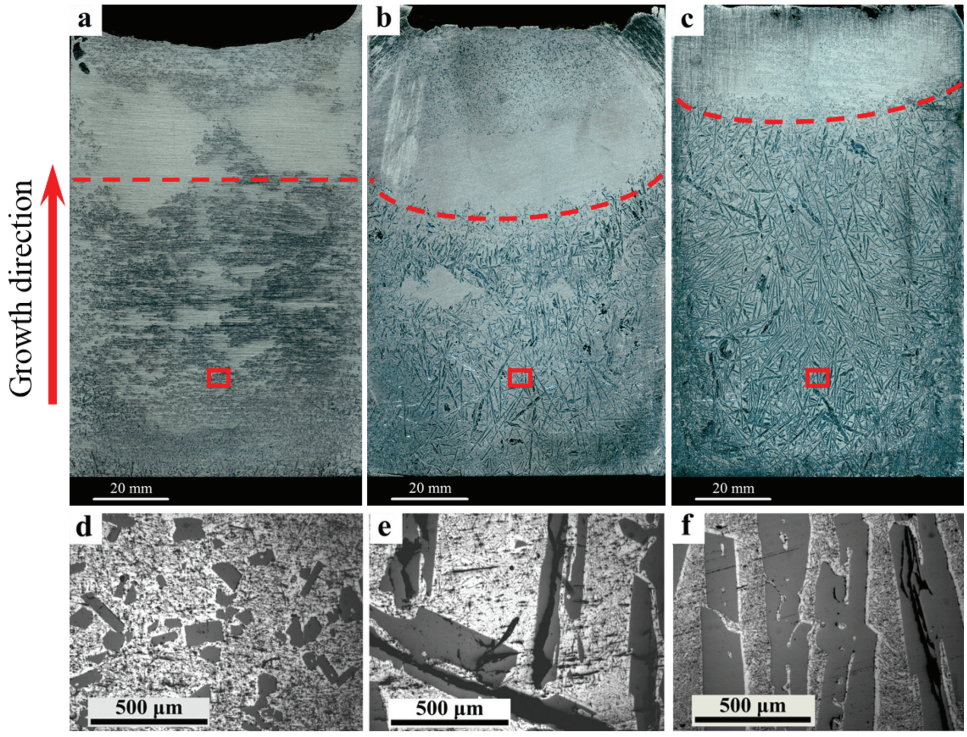

Figure 4: Photographs of vertical cross section of solidified Al-Si ingots. (a) Al-20Si; (b) Al-30Si; (c) Al-40Si; and their corresponding optical microstructures (d), (e) and (f) of the marked area.

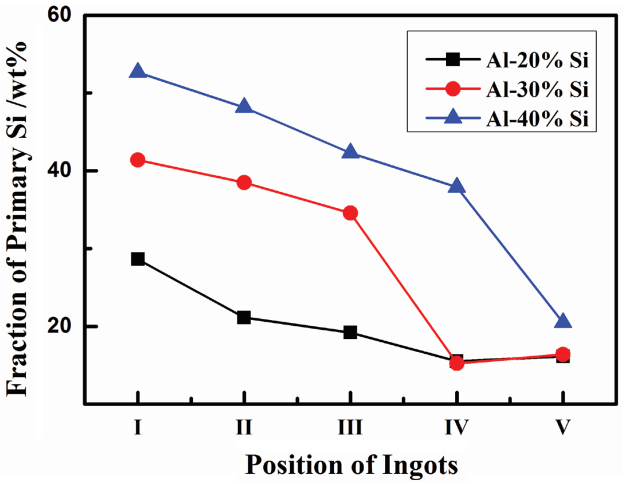

Figure 5: Mass fraction of primary silicon flakes in different parts of ingots.

shown in Figure 4. This is caused by the influence of the impurities, oxides and protective Ar atmosphere.

Distribution of impurities elements

To obtain distribution of B and P in the Al-Si alloys, the concentration profiles of B and P in the primary Si flakes and the eutectic Si powders along the ingot growth direction are constructed from the data of ICP-OES analyses, which is shown in Figure 6.

The concentration of B in the MG-Si raw materials is 25 ppmw. After the Al-Si solvent refining, the B contents in the primary Si flakes were generally less than 10 ppmw, and the content of B in Al-30Si is the lowest in these three samples. This might be related to the TiB_2 particles formed during the solidification process, which needs further study. However, for the eutectic Si powder, B contents were below 10 ppmw only in Al-20Si, all others were about 20 ppmw, which have only little purification effect. In addition, the content of B in the primary Si flakes and the eutectic Si powders fluctuates without obvious trend, which indicates that the directional solidification does not strongly affect the distribution of B.

On the other hand, the concentration of P gradually increases from the bottom to the top of the samples, which reflects the effect of the directional solidification. And it is obvious that the content of P increases gradually when Si content decreases from 40~20 % in Al-Si alloys. The concentrations of P are 43 and 26 ppmw in the MG-Si and the Al of the raw materials, respectively. However, it reaches above 43 ppmw in Al-20Si. This is due to the formation of P containing particles and trapping of these

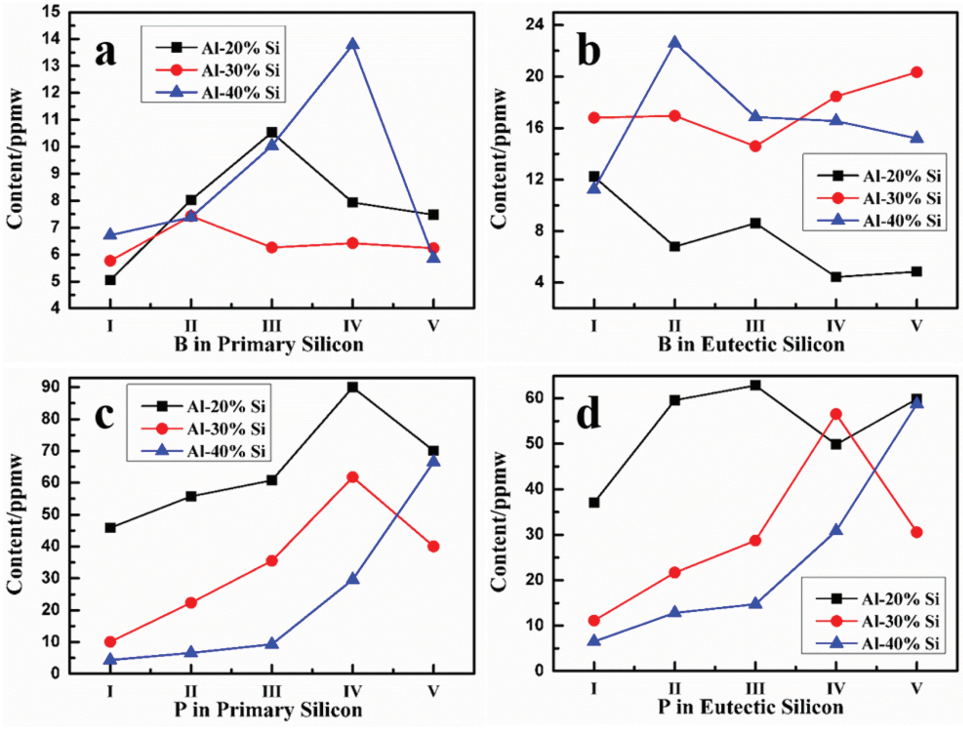

Figure 6: Distribution of B and P in five different parts from bottom to top of ingots. (a) B in primary Si flakes; (b) B in eutectic Si powders; (c) P in primary Si flakes; and (d) P in eutectic Si powders.

particles by the growing primary Si phases at the low solidification temperatures, which is suggested by Li [21] and Ban [24].

The contents of B and P in the primary Si flakes and the eutectic Si powders are less than that in raw materials MG-Si. It can be concluded that B and P are segregated to the Al-Si melt during the forming and growing of the primary Si flakes, and P gradually segregates to the top of ingots during directional solidification. In addition, the contents of B and P have different trends with both Si content in the Al-Si alloys and directional solidification. This could be caused by the following mechanism. The raw materials MG-Si contain some metal element Ti. AlP and TiB_2 particles can form before the primary Si formation during the refining process [24, 25]. The AlP particles can act as nucleation sites for Si phase growth [24], but the TiB_2 particles cannot [25]. So, the alloys with lower solidification temperature contain higher amount of P than B.

Segregation coefficient

An apparent segregation coefficient, k_a, is used to characterize the segregation behavior during the directional solidification process. Assuming that there is a complete mixing of elements in the Al-Si melt and no diffusion in the solidified primary Si flakes, which meets the basic requirement of Gulliver-Scheil model. The content of B and P in the solidified Si can be described by Scheil equation:

$$C_s = k_a C_0 (1 - f_s)^{k_a - 1} \tag{1}$$

where C_s, C_O and f_s are the impurity content in the primary Si flakes, the initial impurity composition in the melt and the fraction of solid, respectively. Considering the law of mass conservation that the total amount of solute in the solid must be equal, the formula is obtained by integration of eq. (1)

$$\int_0^{f_s} k_a C_0 (1 - x)^{k_a - 1} dx = \overline{C_s} f_s \tag{2}$$

then,

$$k_a = log_{1-f_s}\left(1 - \frac{\overline{C_s} f_s}{C_0}\right) \tag{3}$$

where $\overline{C_s}$ and f_s are the average composition of the impurity element in the primary Si and the fraction of the primary Si in the alloy which can be obtained from

Al-Si phase diagram, respectively. In this work, the primary Si flakes mainly gather at the bottom 3/5 of the ingots as shown in Figure 4, so $\overline{C_s}$ could be calculated from the first three data points of impurities in Figure 6.

The apparent segregation coefficient of B and P (k_{aB} and k_{aP}) can be obtained from eq. (3), the results are shown in Figure 7. It can be seen that the apparent segregation coefficients of B and P decrease when the content of Si increase in the Al-Si alloys. On the other hand, the solidification temperature of the alloys rises with increase of Si content in the Al-Si phase diagram (Figure 2(b)). So it can be concluded that apparent segregation coefficients increase with decrease of solidification temperature of the alloys in this work.

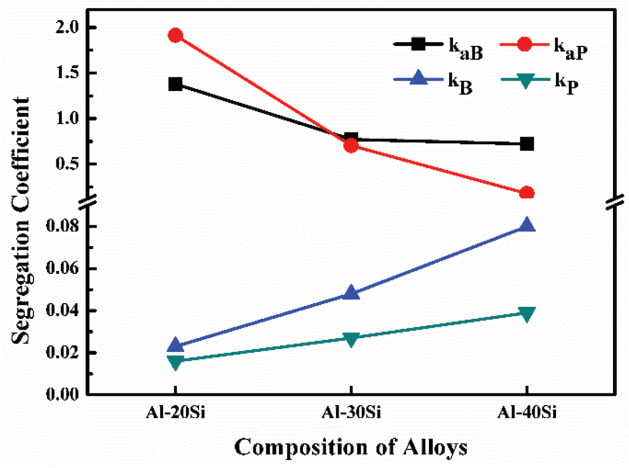

Figure 7: Segregation coefficient of B and P.

Yoshikawa [8, 9] reported that the segregation coefficient of B and P can be expressed by the following equations:

$$\ln k_B = 4.23 - \frac{7300}{T} \tag{4}$$

$$\ln k_P = 1.83 - \frac{5430}{T} \tag{5}$$

where k_B and k_P are the segregation coefficient of B and P, respectively, T is the absolute temperature. For the solidification discussed before is a non-isothermal process, so k_a is actually an average of segregation coefficient $\bar{k}$ of the solidification temperature range, which can be expressed as:

$$\bar{k} = \frac{1}{T_1 - T_0} \int_{T_0}^{T_1} k(T)dT \tag{6}$$

where T_1 is the liquidus temperature, T_0 is the eutectic temperature, and $k(T)$ is the k_B or k_P function of temperature, which is shown in eqs (4) and (5). Bring eqs (4) and (5) into eq (6), the equilibrium segregation coefficient of B and P in Al-Si alloys could be worked out. The comparison with the apparent segregation coefficients of B and P is shown in Figure 7.

The apparent segregation coefficients of B and P are much larger than the equilibrium coefficients and the apparent segregation coefficients of B and P in Al-20Si are even greater than 1. The reasons of the huge numerical difference are as follows. Firstly, the solidification in this work is non-equilibrium and the raw material used in this work is MG-Si and commercial Al. Secondly, the raw material contains high concentration of metal elements such as Fe, Ti and Ca, which would combine to form specific compounds, such as AlP [24, 26] and TiB_2 [25, 27]. Some of these intermetallic compound particles can form before Si phase growth and act as nucleation sites for Si phase growth. Finally, the solidification rate in this work is too fast to let the growing primary Si phases push the compound particles out from them. The compound particles can be trapped easily in this kind of growth condition [28].

In addition, the trends of the apparent segregation coefficients and the equilibrium ones are contradictory. This indicate that kinetic factors have great influence on the apparent segregation coefficients of B and P during directional solidification of the Al-Si alloys, particularly more prominent at the low solidification temperature side. It can be explained by mechanisms of diffusion and convection during the solidification. The schematic drawing of electromagnetic stirring is shown in Figure 8. The viscosity (μ) of the Al-Si melt and the diffusion coefficient (D) of B and P correlate with temperature (T), as shown in eq. (7) and (8).

$$\mu(T) = \mu_0 \exp\left(\frac{E_\mu}{RT}\right) \tag{7}$$

$$D(T) = D_0 \exp\left(-\frac{E_D}{RT}\right) \tag{8}$$

where T is the absolute temperature, μ_0 and D_0 are coefficients, E_μ and E_D are the activation energies and R is the universal gas constant. When the temperature increases, the viscosity of the Al-Si melt decreases and the diffusion coefficient of B and P increases. Thus the amount of convection and diffusion in the melt would be raised. In the hypereutectic Al-Si alloys, when the Si content increases, the liquidus temperature rises. In the meantime, the heating power and therefore the amount of electromagnetic stirring increase, so the amount of convection and diffusion increase with increasing Si

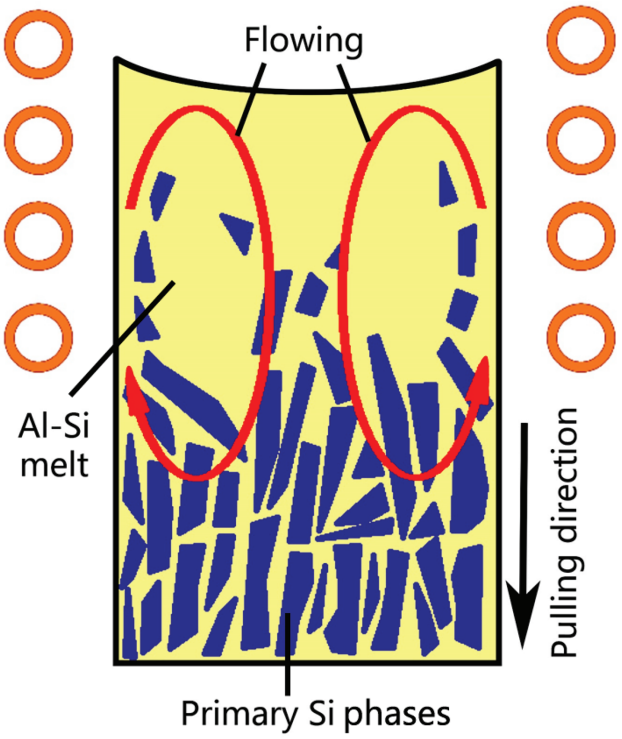

Figure 8: Schematic drawing of electromagnetic stirring mechanism.

content. As a result, the impurity elements B and P can be segregated out of Si effectively when Si content of the Al-Si alloys increases.

Li [20, 21] calculated the apparent segregation coefficient of B and P in Al-30Si alloys at the cooling rate of about 1 mK/s. It is found that the apparent segregation coefficient of P increases with decrease in average solidification temperature, which agrees with the trend in this work. Ban [16] calculated the apparent segregation coefficient of B and P in Al-30Si alloys at the cooling rates of 8.33 and 25 mK/s, respectively. The apparent segregation coefficient of B and P in Al-30Si at different cooling rates are summarized and shown in Figure 9. The apparent segregation coefficients of B and P increase by logarithmic relationship with increase of cooling rate. This also indicates that kinetics has great influence on the apparent segregation coefficients of B and P during silicon purification by the Al-Si solvent refining method. In the Al-Si alloys, B and P need a long time to diffuse from the silicon phase surface to the melt during the formation and growth of the primary Si flakes. Thus the slower cooling rate allows more impurities segregate from the growing primary silicon flake surface to the remaining Al-Si melt.

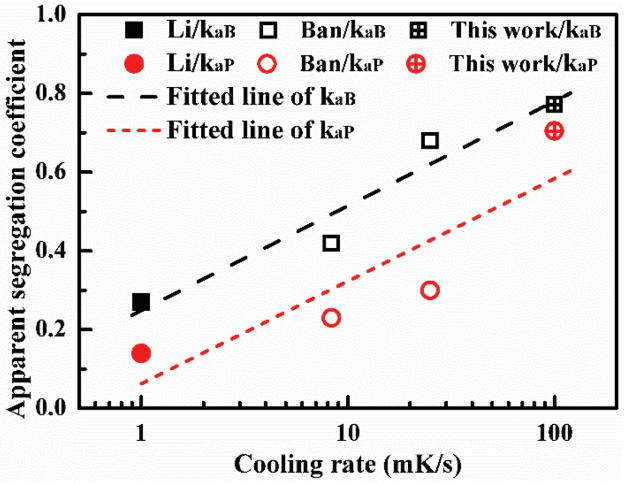

Figure 9: Effect of cooling rate on apparent segregation coefficient.

Conclusions

1. B and P are segregated to the eutectic Al-Si melt during the forming and growing of the primary Si flakes, and P gradually segregate to the top of the ingots during directional solidification.
2. The apparent segregation coefficients of B and P increase with decrease of the solidification temperature of the Al-Si alloys.
3. The kinetic factors have great influence on the apparent segregation coefficients of B and P during directional solidification of the Al-Si alloys. The apparent segregation coefficient decreases with the solidification cooling rate by a logarithmic relationship.

Funding: This work was supported by the Key Lab of Novel Thin Film Solar Cells, Chinese Academy of Sciences and financially supported by National Natural Science Foundation of China (No. 51474201 and No. 51404231); Anhui Provincial Natural Science Foundation (No. 1508085QE81); CPSF-CAS Joint Foundation for Excellent Postdoctoral Fellows (No. 2016LH0017); China Postdoctoral Science Foundation (No. 2014M561846); 100 Talent Program of Chinese Academy of Sciences (No. 2012065).

References

[1] S. Esfahani and M. Barati, Met. Mater. Int., 17 (2011) 1009–1015.

[2] B.P. Lee, H.M. Lee, D.H. Park, J.S. Shin, T.U. Yu and B.M. Moon, Sol. Energy Mater. Sol. Cells, 95 (2011) 56–58.
[3] M. Tanahashi, T. Fujisawa and C. Yamauchi, Metall. Mater. Trans. B, 45B (2014) 629–642.
[4] B.R. Bathey and M.C. Cretella, J. Mater. Sci., 17 (1982) 3077–3096.
[5] M.A. Martorano, J.B.F. Neto, T.S. Oliveira and T.O. Tsubaki, Mater. Sci. Eng. B-Adv., 176 (2011) 217–226.
[6] P.R. Mei, S.P. Moreira, E. Cardoso, A.D.S. Côrtes and F.C. Marques, Sol. Energy Mater. Sol. Cells, 98 (2012) 233–239.
[7] F.A. Trumbore, Bell Syst. Tech. J., 39 (1960) 205–233.
[8] T. Yoshikawa and K. Morita, Sci. Technol. Adv. Mat., 4 (2003) 531–537.
[9] T. Yoshikawa and K. Morita, Metall. Mater. Trans. B, 36B (2005) 731–736.
[10] M. Fang, C.H. Lu, H.X. Lai, L.Q. Huang, J. Chen, W.H. Ma, Z.L. Sheng, J.N. Shen, J.T. Li and X.T. Luo, Mater. Sci. Tech-Lond., 29 (2013) 861–867.
[11] J.W. Li, B.Y. Ban, Y.L. Li, X.L. Bai, T.T. Zhang and J. Chen, Silicon, (2015). doi:10.1007/s12633-014-9269-0.
[12] J.W. Li and Z.C. Guo, J. Cryst. Growth, 394 (2014) 18–23.
[13] J.W. Li, Z.C. Guo, J.C. Li and L.Z. Yu, Silicon, 7 (2015) 239–246.
[14] Y. Nishi, Y. Kang and K. Morita, Mater. Trans., 51 (2010) 1227–1230.
[15] D.H. Lu, Y.H. Jiang, G.S. Guan, R.F. Zhou, Z.H. Li and R. Zhou, J. Mater. Process. Tech., 189 (2007) 13–18.
[16] B.Y. Ban, Y.L. Li, Q.X. Zuo, T.T. Zhang, J. Chen and S.Y. Dai, J. Mater. Process. Tech., 222 (2015) 142–147.
[17] T. Yoshikawa and K. Morita, J. Cryst. Growth, 311 (2009) 776–779.
[18] T. Yoshikawa and K. Morita, ISIJ Int., 45 (2005) 967–971.
[19] H.Y. Xue, G.Q. Lv, W.H. Ma, D.T. Chen and J. Yu, Metall. Mater. Trans. A, 46A (2015) 2922–2932.
[20] Y.L. Li, J. Chen, B.Y. Ban, T.T. Zhang and S.Y. Dai, High Temp. Mat. Proc., 34 (2015) 43–49.
[21] Y.L. Li, B.Y. Ban, J.W. Li, T.T. Zhang, X.L. Bai, J. Chen and S.Y. Dai, Metall. Mater. Trans. B, 46 (2015) 542–544.
[22] X.L. Bai, J. Li, Z. Fu, Y. Li, B. Ban, T. Zhang, Z.J. Peng, C.B. Wang and J. Chen, Int. J. Cast Metal Res., 28 (2015) 269–275.
[23] D.M. Stefanescu, Science and Engineering of Casting Solidification, 2nd ed., Springer, Columbus (2008), pp. 38.
[24] B.Y. Ban, X.L. Bai, J.W. Li, Y.L. Li, J. Chen and S.Y. Dai, Metall. Mater. Trans. B, 46B (2015) 2430–2437.
[25] B.Y. Ban, J.W. Li, X.L. Bai, Q.X. He, J. Chen and S.Y. Dai, J. Alloy Compd., 672 (2016) 489–496.
[26] S. Esfahani and M. Barati, Met. Mater. Int., 17 (2011) 823–829.
[27] T. Yoshikawa, K. Arimura and K. Morita, Metall. Mater. Trans. B, 36B (2005) 837–842.
[28] J. Chen, B.Y. Huang, J.H. Lee, S.J. Choe and Y.T. Lee, J. Mater. Sci. Technol., 15 (1999) 48–52.